Superconducting Dome in a Gate-Tuned Band Insulator

J. T. Ye,[1]* Y. J. Zhang,[1] R. Akashi,[1] M. S. Bahramy,[2] R. Arita,[1,2] Y. Iwasa[1,2]*

A dome-shaped superconducting region appears in the phase diagrams of many unconventional superconductors. In doped band insulators, however, reaching optimal superconductivity by the fine-tuning of carriers has seldom been seen. We report the observation of a superconducting dome in the temperature–carrier density phase diagram of MoS_2, an archetypal band insulator. By quasi-continuous electrostatic carrier doping achieved through a combination of liquid and solid gating, we revealed a large enhancement in the transition temperature T_c occurring at optimal doping in the chemically inaccessible low–carrier density regime. This observation indicates that the superconducting dome may arise even in doped band insulators.

In many unconventional superconductors (*1*–*3*), the transition temperature T_c has a maximum as a function of external parameters such as chemical doping or pressure; in cuprate families, this so-called superconducting dome arises upon the chemical doping of the parent Mott insulator (*1*). In band insulators, similar behavior was observed at low carrier densities (*4*) where superconductivity is usually not favorable because of the low density of states (DOS) (*4*, *5*). Except in certain cases (*4*, *6*), however, using chemical doping to achieve low carrier densities results in nonuniformity or phase separation. Other systems exhibiting optimal doping of the superconducting state include two-dimensional (2D) electron systems at surfaces and interfaces, whose phase diagrams may be explored by applying electric fields (*7*–*9*). In recent years, this electrostatic carrier doping has been effectively implemented by using ionic liquids to form an electrical double layer (EDL) of high capacitance (*10*–*12*). This method has produced carrier densities that span the superconducting dome in high-T_c cuprates (*13*, *14*) and may be an effective tool to access exotic superconducting states in other materials.

We chose a typical band insulator, MoS_2, because the high mobility found in its solid-state transistor operations (*15*) suggests that interesting basic physical properties may be revealed by using the EDL dielectrics (*11*, *16*–*18*). To make our devices, we isolated thin flakes of MoS_2 from a bulk 2*H*-type single crystal (Fig. 1A) by the Scotch tape method widely used in graphene research (*19*, *20*) and transferred them onto the surface of HfO_2 grown by atomic layer deposition on a Nb-doped $SrTiO_3$ substrate. We selected atomically flat thin flakes by examining their optical micrographs (*21*) and patterned them into a Hall bar configuration (Fig. 1B), which acts as a transistor channel (*11*, *16*). A droplet of ionic liquid (DEME-TSFI) (*21*) was applied onto the surface of the thin flake covering the side gate electrode (Fig. 1C). A voltage applied between the thus formed liquid gate (LG) and the channel drives either anions or cations onto the channel surface under positive or negative bias, respectively. The ions and induced carriers (~10^{14} cm^{-2}) right beneath form an equivalent capacitance of ~10 μF/cm^2, large enough for inducing superconductivity at the interface (*10*–*14*). In addition, we were able to modulate the carrier density (to ~10^{13} cm^{-2}) using a high-*k* dielectric (HfO_2) back gate (BG), which remains effective after the freezing of the ion motion at a temperature below ~200 K. For carriers induced at the top surface of the MoS_2 flake by the LG, the effective BG capacitance is affected by two layers of dielectrics: HfO_2 and the bulk of MoS_2 flake. Using this double gating method, we could access a large range of carrier densities n_{2D} quasi-continuously and precisely, thereby avoiding the staging effect (*22*), even in the low-density

[1]Quantum-Phase Electronics Center and Department of Applied Physics, University of Tokyo, 7-3-1 Hongo, Bunkyo-ku, Tokyo 113-8656, Japan. [2]Correlated Electron Research Group, RIKEN, Hirosawa 2-1, Wako 351-0198, Japan.

*To whom correspondence should be addressed. E-mail: yejianting@ap.t.u-tokyo.ac.jp (J.T.Y.); iwasa@ap.t.u-tokyo.ac.jp (Y.I.)

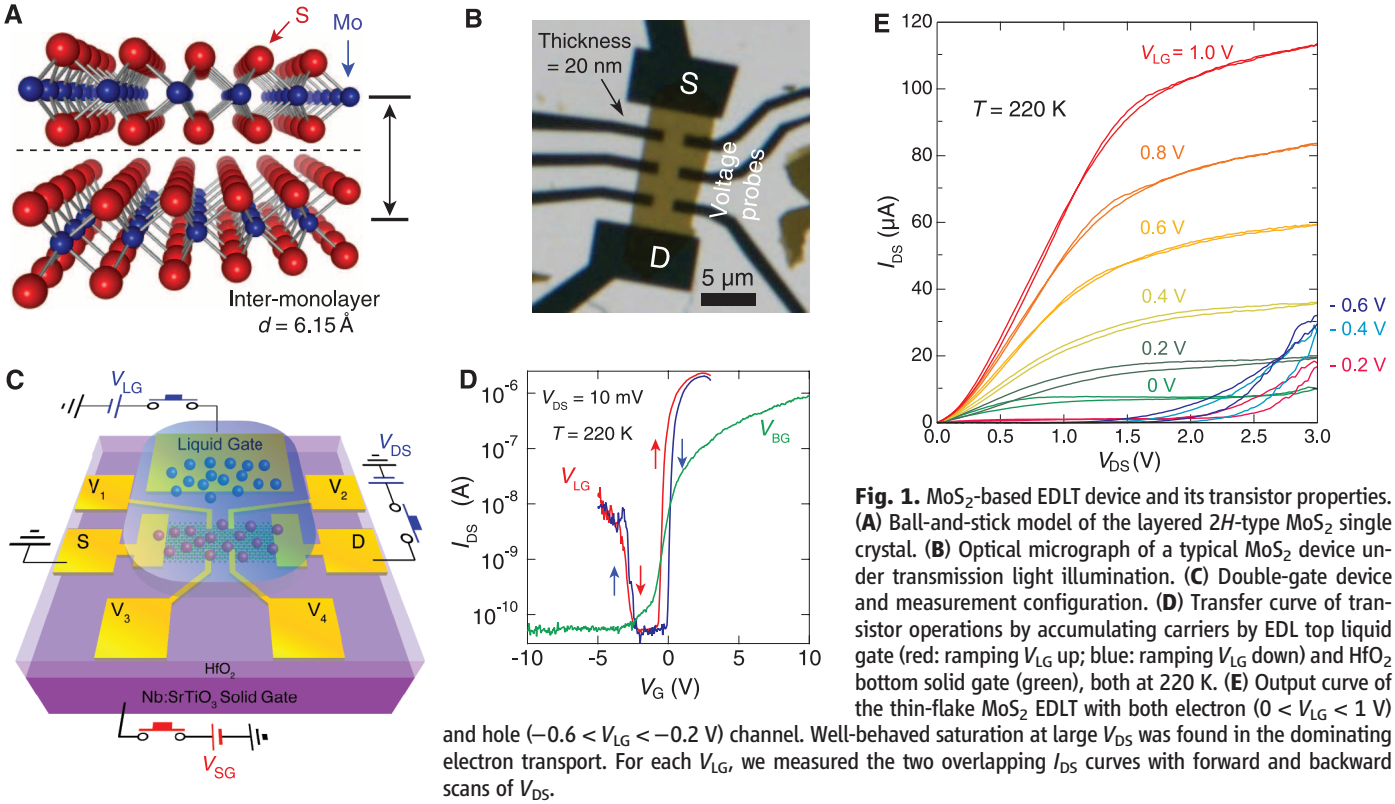

Fig. 1. MoS_2-based EDLT device and its transistor properties. (**A**) Ball-and-stick model of the layered 2*H*-type MoS_2 single crystal. (**B**) Optical micrograph of a typical MoS_2 device under transmission light illumination. (**C**) Double-gate device and measurement configuration. (**D**) Transfer curve of transistor operations by accumulating carriers by EDL top liquid gate (red: ramping V_{LG} up; blue: ramping V_{LG} down) and HfO_2 bottom solid gate (green), both at 220 K. (**E**) Output curve of the thin-flake MoS_2 EDLT with both electron ($0 < V_{LG} < 1$ V) and hole ($-0.6 < V_{LG} < -0.2$ V) channel. Well-behaved saturation at large V_{DS} was found in the dominating electron transport. For each V_{LG}, we measured the two overlapping I_{DS} curves with forward and backward scans of V_{DS}.

regime where chemical doping is plagued by nonuniformity.

Figure 1D shows the transfer curves of a typical double-gate device at 220 K with a source-drain voltage V_{DS} = 10 mV. For the *n*-channel conduction, an on/off ratio of $>10^4$ was reached for biasing with either the liquid ionic gate (V_{LG}) or the high-*k* back gate (V_{BG}), with a channel resistance $R_{DS} > 1$ gigohm in the off state. Compared with the BG, the LG not only had 10 times the gate efficiency (the change of channel current versus gate voltage $\frac{\Delta I_{DS}}{\Delta V_G}$), but also created an additional p-channel when a negative V_G was applied. This ambipolar transport indicates that the LG is effective in shifting the Fermi level E_F to access both the valence and conduction bands (*16*). An enhanced p-channel with more balanced ambipolar transport could be found in flakes with less intrinsic electron doping (sulfur deficiency), where the barely metallic state in the p-channel was still far from reaching hole superconductivity (*16*). To confirm the electrostatic operation of LG, we performed a transfer curve measurement with fast gate bias cycles (fig. S1). The possibility of a chemical reaction was ruled out by repeatability and a negligible (~1 nA) leak current I_G, as well as a persistent off state (> 1 gigohm). The I_{DS} versus V_{DS} characteristic in the output operation (Fig. 1E) of a typical MoS_2 EDL transistor (EDLT) corroborates the more pronounced n-channel ($0 < V_{LG} < 1$ V) than p-channel operation ($-0.6 < V_{LG} < -0.2$V), consistent with the transfer characteristics. Compared with the n-channel operation observed in monolayer devices (*15*), the more pronounced saturation at high V_{DS} indicates well-behaved transistor operation.

After introducing carriers onto the channel surface at 220 K with different liquid-gate biases V_{LG}, we measured the four-terminal sheet resistance R_s as a function of temperature *T* when the device was being cooled down to 2 K (Fig. 2A). At gate biases $V_{LG} < 1$ V, we observed a negative temperature derivative of R_s (dR_s/dT) for insulating states. The increase of dR_s/dT with V_{LG} indicates the gradual formation of degenerate carriers and enhanced mobility at low temperatures. The channel surface shows metallic transport (positive dR_s/dT) at $V_{LG} \geq 1$ V. The enhancement of metallicity continues with further increase of V_{LG}, and superconductivity emerges at V_{LG} = 4 V. The transition temperature T_c shows clear V_{LG}

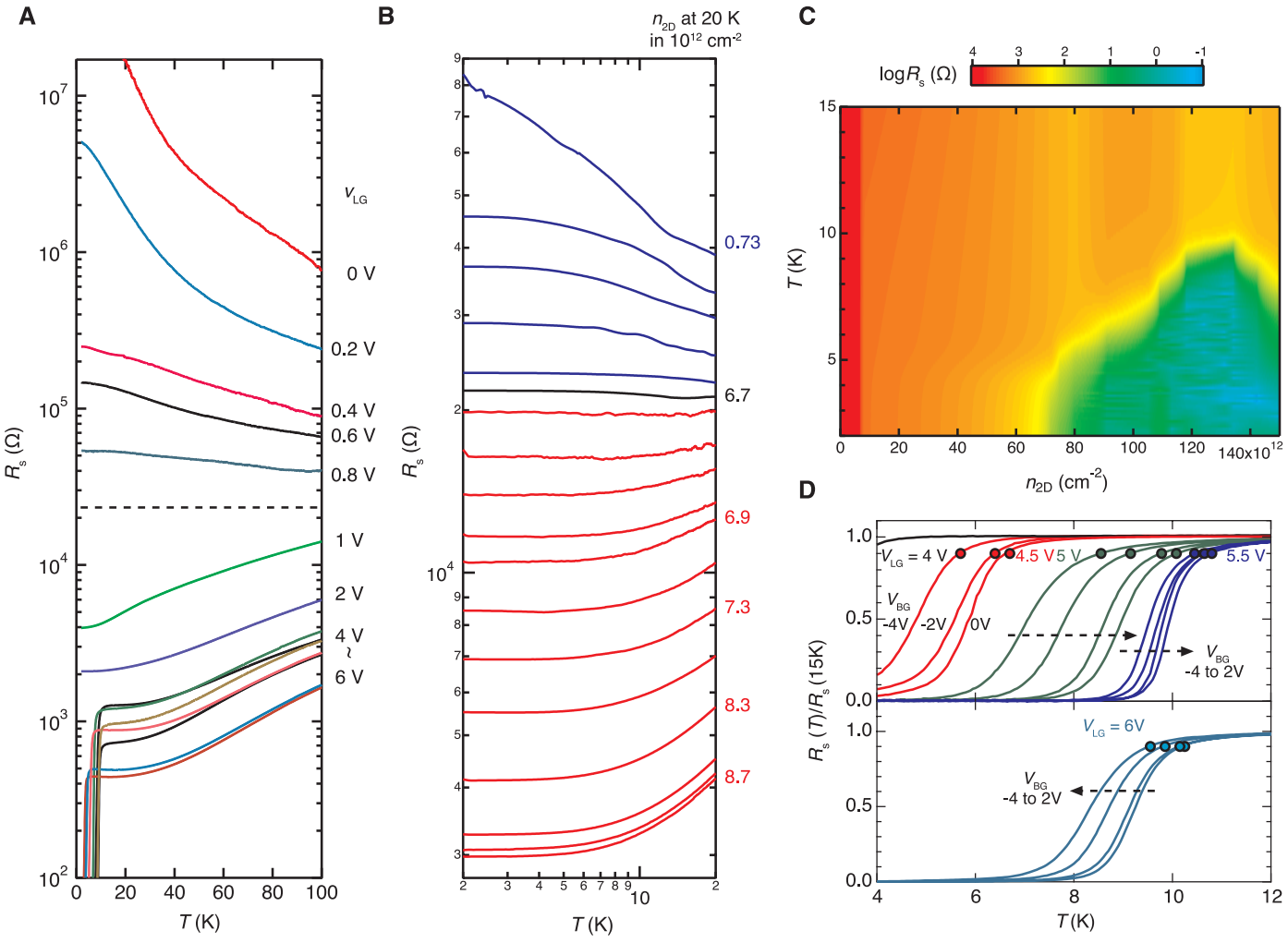

Fig. 2. Transport properties of the thin-flake MoS_2 EDLT. (**A**) Temperature dependence of the channel sheet resistance R_s at different V_{LG} gate biases ranging from 0 to 6 V (indicated on the right). (**B**) Temperature dependence of the channel sheet resistance R_s at V_{LG} = 1 V and different V_{BG}'s showing a metal-insulator transition at $n_{2D} = 6.7 \times 10^{12}$ cm^{-2}. For each V_{BG}, we marked the corresponding n_{2D} measured by the Hall effect at 20 K. (**C**) Phase diagram showing the evolution of different electronic phases as a function of carrier density n_{2D}. The phase diagram shows an insulating ($n_{2D} < 6.7 \times 10^{12}$ cm^{-2}), a metallic ($6.7 \times 10^{12} < n_{2D} < 6.8 \times 10^{13}$ cm^{-2}), and a dome-like superconducting phase ($n_{2D} > 6.8 \times 10^{13}$ cm^{-2}), where the color corresponds to the logarithm of the sheet resistance R_s (Ω). (**D**) Normalized superconducting transition R_s/R_s (15K) as a function of temperature for different gate voltages. The T_c is marked as a circle at 90% of the total transition. Both V_{LG} and V_{BG} are varied; for a given V_{LG}, we show the evolution of the transition with increasing V_{BG}. All data corresponding to the same V_{LG} are shown with the same color. The dashed arrows indicate the order of increasing V_{BG} from −4 to 2 V in ΔV_{BG} = 2 V. (Upper panel) For V_{LG} between 4 and 5.5 V, T_c increased with increasing V_{BG}; (bottom panel) for V_{LG} = 6 V, T_c decreased with increasing V_{BG} because the corresponding n_{2D} had reached the peak of the superconducting dome.

dependence until V_{LG} reaches 6 V, the maximum voltage used in our experiment. Similar field-induced superconductivity was reported recently by Taniguchi *et al*. (*23*).

For the metallic states at V_{LG} = 1 V, we switched on the solid back gate to study the metal insulator transition (MIT) by a precise control of the transport with 18 different n_{2D} values ($7.3 \times 10^{11} < n_{2D} < 8.7 \times 10^{12}$ cm^{-2}) measured by the Hall effect at 20 K (Fig. 2B). A transition between the insulating (blue) and metallic (red) transport was clearly separated by a critical resistance R_c = 21.7 kilohm (separatrix, black line) at $n_c = 6.7 \times 10^{12}$ cm^{-2}, close to the quantum resistance h/e^2, consistent with MITs found in other 2D systems (*24*). A Hall mobility of $\mu_H \sim 240$ cm^2/V s at $n_{2D} = 8.7 \times 10^{12}$ cm^{-2} is comparable to the bulk value (*25*), supporting our choice of (~20 nm thick) flakes instead of monolayers, where ripples might lower the mobility (*26*, *27*). After the formation of metallic states, increasing the gate bias also creates a growing perpendicular surface electric field E_s, inducing spin-orbit interaction, which corroborates the 2D nature of MoS_2 interface (*21*, *28*). Varying both V_{LG} and V_{BG}, we quasi-continuously mapped log R_s in the n_{2D} and T plane (Fig. 2C). This enables a detailed study of the full superconducting phase induced by the field effect in a pristine compound, avoiding a nonuniform dopant distribution or phase separation. At several fixed values of V_{LG}, we manipulated T_c by varying V_{BG} (Fig. 2D).

Figure 3A shows a superconducting phase diagram of MoS_2 as a function of n_{2D} measured by Hall effect at 20 K. As estimated from the Thomas-Fermi screening length for $n_{2D} \sim 10^{14}$ cm^{-2}, we assumed that the carriers are accumulated in a half of one unit cell, 6.15 Å (a monolayer). Notably, this value of n_{2D} can be regarded as the upper limit to the estimate of n_{2D} when we unify our phase diagram with that of alkali metal–intercalated 2*H*-MoS_2 in Fig. 3A (*29*, *30*). The superconductivity sharply appears at $n_{2D} = 6.8 \times 10^{13}$ cm^{-2}, then saturates after reaching a maximum T_c = 10.8 K at $n_{2D} = 1.2 \times 10^{14}$ cm^{-2}, followed by a decrease in T_c at larger n_{2D}; this results in a dome-like superconducting state. We defined T_c as the temperature at which R_s reaches 90% of its normal state value. At the onset of the superconducting phase, the critical behavior near the quantum critical point could be well fitted with $T \propto (n_{2D} - n_0)^{z\nu}$, where $z\nu = 0.6$ (fig. S4), in a manner similar to that for $LaAlO_3/SrTiO_3$ interfaces (*7*). This is also consistent with $z\nu = 0.5 \sim 0.6$ found in boron-doped diamond, where a comparable T_c was observed (*31*).

In the combined phase diagram, which includes the chemically doped MoS_2 (*29*, *30*), the field-induced phase showed enhanced T_c (~40% higher than the maximum T_c found in Cs_xMoS_2) at a much lower n_{2D} (Fig. 3A). The maximum T_c is also well above that of $NbSe_2$ (~7 K), which was thought to be the highest T_c in transition-metal dichalcogenides. That the field-induced phase appears with an enhanced T_c at a much lower n_{2D} with respect to the alkali metal–doped compounds confirms the effectiveness of searching for different regions of carrier concentrations in doped semiconductors. It appears that the decrease in T_c connects smoothly to the region of bulk superconductivity for alkali metal–doped MoS_2 compounds.

To understand these superconducting features found in MoS_2 EDLT, we calculated its electronic structure for both monolayer and bulk (*21*). Figure 3B shows the DOS spectrum for the electron-doped monolayer MoS_2, which mimics the gate-induced charge accumulation layer at large carrier densities of $\sim 10^{14}$ cm^{-2}. The conduction band edge consists predominantly of the d_{z^2} orbital of Mo. Reflecting the 2D nature of the monolayer, the DOS is nearly flat in the region of $6.8 \times 10^{13} < n_{2D} < 1.2 \times 10^{14}$ cm^{-2}, where superconductivity sharply sets in and reaches the maximum T_c, corresponding to an E_F shift of 0.25 eV from the band edge (*21*). The DOS continues to increase with n_{2D} owing to the contribution from additional $d_{x^2-y^2}$ and d_{xy} orbitals, indicating that the decrease in T_c above 1.2×10^{14} cm^{-2} is not simply controlled by the change in the DOS.

Such a decrease in T_c with increasing carrier density was first recognized in Na-doped WO_3 and was attributed to phonon softening from a structural transition observed in the vicinity of the superconducting phase (*32*). However, the phonon softening scenario should not apply to MoS_2 because its structural transition occurs at an order of magnitude higher n_{2D} (*33*). A similar superconducting dome with a quantum critical point has been recently observed in electric-field–controlled interface superconductivity such as in $LaAlO_3/SrTiO_3$ (*7*) and $KTaO_3$ (*12*). Thus, it is possible that a more universal, non–material-

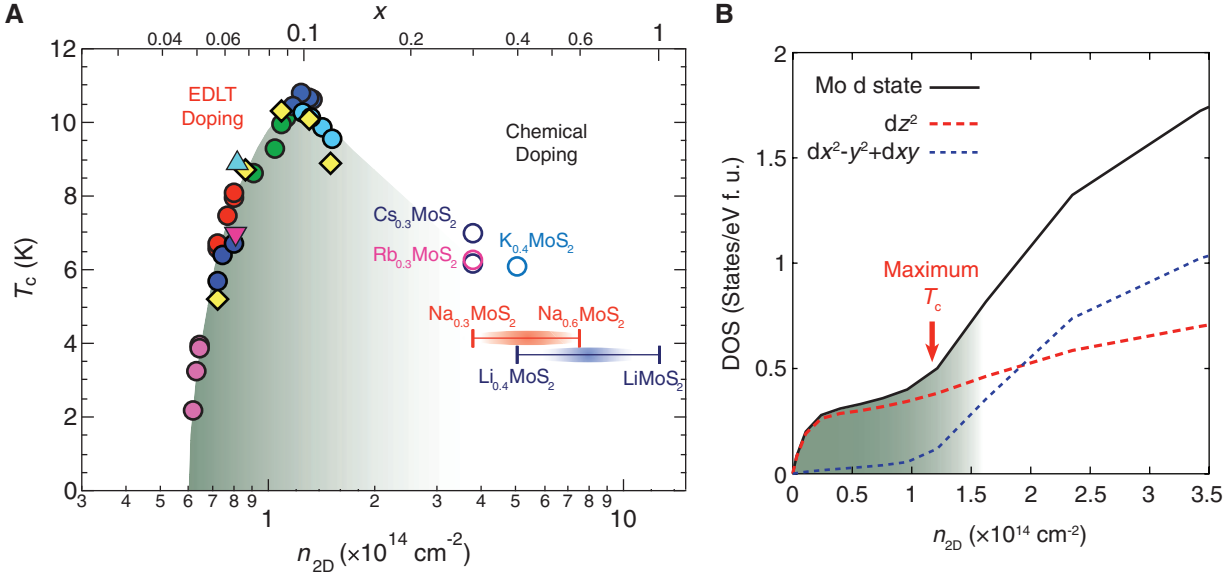

Fig. 3. Phase diagram and band calculation of electron-doped MoS_2. (**A**) Unified phase diagram of superconductivity of both electrostatically and chemically doped MoS_2 as a function of doping concentration x (upper horizontal axis) and carrier density n_{2D} (bottom horizontal axis). The field-induced superconducting data were from four different samples, each marked with a differently shaped filled symbol. Filled circles of the same color correspond to the superconducting states at a fixed V_{LG} but different V_{BG}'s. Open circles show the T_c of MoS_2 chemically intercalated with different alkali metal dopants. Solid bars denote the range of doping showing the same T_c. The structure of all intercalated compounds is 2*H*-type within the indicated carrier density region. (**B**) Calculated DOS of MoS_2. The field-induced carriers mainly occupy the 4d state of Mo, covering the n_{2D} region indicated by the shaded green area. The red arrow locates the n_{2D} where the maximum T_c was observed.

specific model exists for the superconducting phase diagram in doped band insulators at dilute carrier densities.

References and Notes

1. P. A. Lee, N. Nagaosa, X. G. Wen, *Rev. Mod. Phys.* **78**, 17 (2006).
2. R. E. Schaak, T. Klimczuk, M. L. Foo, R. J. Cava, *Nature* **424**, 527 (2003).
3. Y. Takabayashi *et al.*, *Science* **323**, 1585 (2009).
4. C. S. Koonce, M. L. Cohen, J. F. Schooley, W. R. Hosler, E. R. Pfeiffer, *Phys. Rev.* **163**, 380 (1967).
5. J. F. Schooley *et al.*, *Phys. Rev. Lett.* **14**, 305 (1965).
6. Y. Taguchi, A. Kitora, Y. Iwasa, *Phys. Rev. Lett.* **97**, 107001 (2006).
7. A. D. Caviglia *et al.*, *Nature* **456**, 624 (2008).
8. N. Reyren *et al.*, *Science* **317**, 1196 (2007).
9. C. H. Ahn *et al.*, *Rev. Mod. Phys.* **78**, 1185 (2006).
10. K. Ueno *et al.*, *Nat. Mater.* **7**, 855 (2008).
11. J. T. Ye *et al.*, *Nat. Mater.* **9**, 125 (2010).
12. K. Ueno *et al.*, *Nat. Nanotechnol.* **6**, 408 (2011).
13. A. T. Bollinger *et al.*, *Nature* **472**, 458 (2011).
14. X. Leng, J. Garcia-Barriocanal, S. Bose, Y. Lee, A. M. Goldman, *Phys. Rev. Lett.* **107**, 027001 (2011).
15. B. Radisavljevic, A. Radenovic, J. Brivio, V. Giacometti, A. Kis, *Nat. Nanotechnol.* **6**, 147 (2011).
16. Y. Zhang, J. Ye, Y. Matsuhashi, Y. Iwasa, *Nano Lett.* **12**, 1136 (2012).
17. J. T. Ye *et al.*, *Proc. Natl. Acad. Sci. U.S.A.* **108**, 13002 (2011).
18. J. G. Checkelsky, J. T. Ye, Y. Onose, Y. Iwasa, Y. Tokura, *Nat. Phys.* **8**, 729 (2012).
19. K. S. Novoselov *et al.*, *Science* **306**, 666 (2004).
20. K. S. Novoselov *et al.*, *Proc. Natl. Acad. Sci. U.S.A.* **102**, 10451 (2005).
21. Information on materials and methods is available in the supplementary materials on *Science* Online.
22. R. H. Friend, A. D. Yoffe, *Adv. Phys.* **36**, 1 (1987).
23. K. Taniguchi, A. Matsumoto, H. Shimotani, H. Takagi, *Appl. Phys. Lett.* **101**, 042603 (2012).
24. E. Abrahams, S. V. Kravchenko, M. P. Sarachik, *Rev. Mod. Phys.* **73**, 251 (2001).
25. R. Fivaz, E. Mooser, *Phys. Rev.* **163**, 743 (1967).
26. J. Brivio, D. T. L. Alexander, A. Kis, *Nano Lett.* **11**, 5148 (2011).
27. W. S. Yun, S. W. Han, S. C. Hong, I. G. Kim, J. D. Lee, *Phys. Rev. B* **85**, 033305 (2012).
28. A. D. Caviglia *et al.*, *Phys. Rev. Lett.* **104**, 126803 (2010).
29. J. A. Woollam, R. B. Somoano, *Mater. Sci. Eng.* **31**, 289 (1977).
30. R. B. Somoano, V. Hadek, A. Rembaum, S. Samson, J. A. Woollam, *J. Chem. Phys.* **62**, 1068 (1975).
31. T. Klein *et al.*, *Phys. Rev. B* **75**, 165313 (2007).
32. H. R. Shanks, *Solid State Commun.* **15**, 753 (1974).
33. R. B. Somoano, V. Hadek, A. Rembaum, *J. Chem. Phys.* **58**, 697 (1973).

Acknowledgments: We thank Y. Takada and A. Bianconi for fruitful discussions and M. Nakano and Y. Kasahara for experimental help. This work was supported by a Grant-in-Aid for Scientific Research (S) (no. 21224009) from Japan and Strategic International Collaborative Research Program (SICORP), Japan Science and Technology Agency. M.S.B., R.A., and Y.I. were supported by the Japan Society for the Promotion of Science through its Funding Program for World-Leading Innovative R&D on Science and Technology (FIRST Program). Y.I. received additional funding from SICORP, Japan Science and Technology Agency.

Supplementary Materials

www.sciencemag.org/cgi/content/full/338/6111/1193/DC1
Materials and Methods
Figs. S1 to S5
References (*34*–*47*)

26 July 2012; accepted 17 October 2012
10.1126/science.1228006

Formation of Regular Satellites from Ancient Massive Rings in the Solar System

A. Crida[1]* and S. Charnoz[2,3]

When a planetary tidal disk—like Saturn's rings—spreads beyond the Roche radius (inside which planetary tides prevent aggregation), satellites form and migrate away. Here, we show that most regular satellites in the solar system probably formed in this way. According to our analytical model, when the spreading is slow, a retinue of satellites appear with masses increasing with distance to the Roche radius, in excellent agreement with Saturn's, Uranus', and Neptune's satellite systems. This suggests that Uranus and Neptune used to have massive rings that disappeared to give birth to most of their regular satellites. When the spreading is fast, only one large satellite forms, as was the case for Pluto and Earth. This conceptually bridges the gap between terrestrial and giant planet systems.

Satellites are generally thought to form concurrently with a giant planet, in a large circumplanetary gaseous disk where there is inflow of solids. Two competing models exist in the literature (*1*–*4*), in which solids aggregate to form satellites that can migrate in the gas (and possibly be lost) before the gas dissipates. These models have their pros and cons, but none can explain the surprising orbital architecture of Saturn's, Uranus', and Neptune's satellite systems, where the smallest bodies accumulate at a distance from the planet that is twice its radius (the Roche radius), and their masses increase with distance starting from this point (Fig. 1A). Moreover, in the frame of a circumplanetary gas disk, Uranus' satellites should orbit in the ecliptic plane, and not the equatorial plane of the tilted planet (*5*). Also, Uranus and Neptune might be too light to have retained a massive enough gaseous disk (*6*). These considerations suggest that an alternative model is needed, to explain at least the origin of the giant planets' innermost satellites.

Here, we consider a disk of solid material around a planet, similar to Saturn's rings, wherein planetary tides prevent aggregation within the Roche radius r_R (*7*) [supplementary text 1 (SM 1)]. It is known that such a tidal disk will spread (*8*). Thus, the normalized disk lifetime can be defined by $\tau_{disk} = M_{disk}/FT_R$, where F is the mass flow through r_R, T_R is the orbital period at r_R, and $M_{disk} = \pi\Sigma r_R^2$ is the disk's mass (Σ being the surface density). Using a prescription for the viscosity based on self-gravity and mutual collisions (*9*), one finds

$$\tau_{disk} = 0.0425/D^2 \quad (1)$$

where $D = M_{disk}/M_p$ and M_p is the planet's mass (SM 2.2.1).

As material migrates beyond r_R, new moons form (*10*, *11*). They are then repelled by the tidal disk through resonant angular momentum exchange and migrate outward as they grow. A satellite of mass M orbiting outside a tidal disk experiences a positive gravitational torque (*12*)

$$\Gamma = (32\pi^2/27)q^2\Sigma r_R^4 T_R^{-2}\Delta^{-3} \quad (2)$$

where $q = M/M_p$, $\Delta = (r - r_R)/r_R$, and r is the orbital radius. Thus, it migrates outward at a rate (SM 2.1)

$$d\Delta/dt = (2^5/3^3)qDT_R^{-1}\Delta^{-3} \quad (3)$$

The migration rate increases with mass-ratio q and decreases with distance Δ. Based on the restricted three-body problem, we assume that a satellite accretes everything within 2 Hill radii, r_H, from its orbit (*13*, *14*) [$r_H = r(q/3)^{1/3}$]. Thus, as a tidal disk spreads, a competition takes place between accretion and migration. We assume that the satellites do not perturb each other's orbit or the disk (SM 10), that $\Delta << 1$, and that D and τ_{disk} (thus F and Σ) are constant. We find from our analytical model (SM) that moon accretion proceeds in three steps, corresponding to three different regimes of accretion.

When the disk starts spreading, a single moon forms at the disk's edge (moon 1). As long as $\Delta < 2r_H/r$, it will directly accrete the material flowing through r_R and grow linearly with time, while migrating outward. This is the "continuous regime" (Fig. 2A, SM 3). Integrating Eq. 3 with $M = Ft$, one finds that the condition $\Delta < 2r_H/r$ holds until

$$\Delta = \Delta_c = (3/\tau_{disk})^{1/2} \quad (4)$$

$$q = q_c = \sim 2\tau_{disk}^{-3/2}$$

Using Eq. 1, one finds $\Delta_c = 8.4D$, occurring after ~10 orbits (SM 3.1).

[1]Laboratoire Lagrange UMR 7293, Université de Nice Sophia–antipolis, CNRS, Observatoire de la Côte d'Azur, BP4229, 06304 Nice Cedex 4, France. [2]Université Paris Diderot, Sorbonne Paris Cité, Laboratoire AIM, CEA -Service d'Astrophysique 91191 Gif-sur-Yvette Cedex France. [3]Institut Universitaire de France, 103 bd Saint Michel, 75005 Paris, France.

*To whom correspondence should be addressed. E-mail: crida@oca.eu.

Superconducting Dome in a Gate-Tuned Band Insulator
J. T. Ye, Y. J. Zhang, R. Akashi, M. S. Bahramy, R. Arita and Y. Iwasa (November 29, 2012)
Science **338** (6111), 1193-1196. [doi: 10.1126/science.1228006]

Editor's Summary

What Do You Know? A Dome

The superconducting dome—the appearance of a maximum in the transition temperature as a function of a tuning parameter—has been observed in compounds such as cuprates, pnictides, and heavy fermion materials and is thought of as a signature of unconventional superconductivity. **Ye *et al.*** (p. 1193) used a liquid gating technique combined with back gating to finely tune the carrier density in the band insulator MoS_2, which allowed them to observe the formation of a dome. The unexpected finding awaits theoretical explanation but may suggest that the appearance of an optimal carrier density may be a more common occurrence than was previously thought.

Science (print ISSN 0036-8075; online ISSN 1095-9203) is published weekly, except the last week in December, by the American Association for the Advancement of Science, 1200 New York Avenue NW, Washington, DC 20005.